STRUCTURE AND DYNAMICS OF ION TRANSPORT THROUGH GRAMICIDIN A

DONALD H. J. MACKAY, PETER H. BERENS, AND KENT R. WILSON
Department of Chemistry, University of California, San Diego, La Jolla, California 92093

ARNOLD T. HAGLER
Agouron Institute, La Jolla, California 92037

ABSTRACT Molecular dynamics calculations in which all atoms were allowed to move were performed on a water-filled ion channel of the polypeptide dimer gramicidin A (~600 atoms total) in the head-to-head Urry model conformation. Comparisons were made among nine simulations in which four different ions (lithium, sodium, potassium, and cesium) were each placed at two different locations in the channel as well as a reference simulation with only water present. Each simulation lasted for 5 ps and was carried out at ~300 K. The structure and dynamics of the peptide and interior waters were found to depend strongly on the ion tested and upon its location along the pore. Speculations on the solution and diffusion of ions in gramicidin are offered based on the observations in our model that smaller ions tended to lie off axis and to distort the positions of the carbonyl oxygens more to achieve proper solvation and that the monomer-monomer junction was more distortable than the center of the monomer. With the potential energy surface used, the unique properties of the linear chain of interior water molecules were found to be important for optimal solvation of the various ions. Strongly correlated motions persisting over 25 Å among the waters in the interior single-file column were observed.

INTRODUCTION

Ion channels are a widely used biological mechanism, which are employed not only to allow certain ions to cross membranes while blocking others, but also to allow signals to be transmitted quickly along and across membranes (1). The understanding of the microscopic mechanism of ion transport and selectivity in channels is a logical step along the way toward understanding other more complex mechanisms, i.e., (*a*) gating of ion channels, (*b*) passive transport of polar molecules across membranes, and (*c*) active transport of ions and molecules across membranes (recognizing, of course, that mechanisms of active transport may not necessarily resemble mechanisms of passive transport). However, while these complex mechanisms are very important, the simpler question of how ions actually navigate with the help of a channel across the dielectric barrier of lipid bilayers is still poorly understood.

Gramicidin A is a polypeptide containing 15 alternating D-L amino acids (see Figs. 1–4)

HCO—*L*—Val[1]—Gly[2]—*L*—Ala[3]—*D*—Leu[4]—*L*—Ala[5]
—*D*—Val[6]—*L*—Val[7]—*D*—Val[8]—*L*—Trp[9]—*D*—Leu[10]—
L—Trp[11]—*D*—Leu[12]—*L*—Trp[13]—*D*—Leu[14]—*L*—Trp[15]
—$NHCH_2CH_2OH$

Address all correspondence to K. R. Wilson.

that forms ion conducting channels across a wide variety of membranes (2,3). Fig. 1 provides a schematic representation of gramicidin dimers embedded in lipid bilayers separating water interfaces. The ions and waters are shown in various locations in the pore forming an internal one-dimensional liquid. It has been noted that the function of gramicidin in nature may not necessarily be as an ion channel, but rather as a cofactor in RNA synthesis (4,5). However, it certainly acts as an ion channel when placed in membranes and as such can serve as a useful model for studying the interrelation of structure, dynamics, and biological action.

Much effort, both experimental and theoretical, has been devoted to discovering the structure and properties of the ion conducting form of gramicidin. For a recent review, see Andersen (6). From osmotic and diffusional permeability measurements, it appears that the channel holds a single file of five to six waters (7), although electrokinetic experiments (streaming potentials and electroosmosis) suggest that seven to nine waters are coupled to the transport of ions at low ion concentrations (8,9). Only small (generally monatomic) monovalent cations can pass through the pore (2, 10–12). There have been low resolution x-ray studies on gramicidin (13) although the relevance of the crystal structure to the conformation of gramicidin in membranes is uncertain due to the variety of conformations available to gramicidin in various solvents (14–16). Evidence to date supports a model first proposed

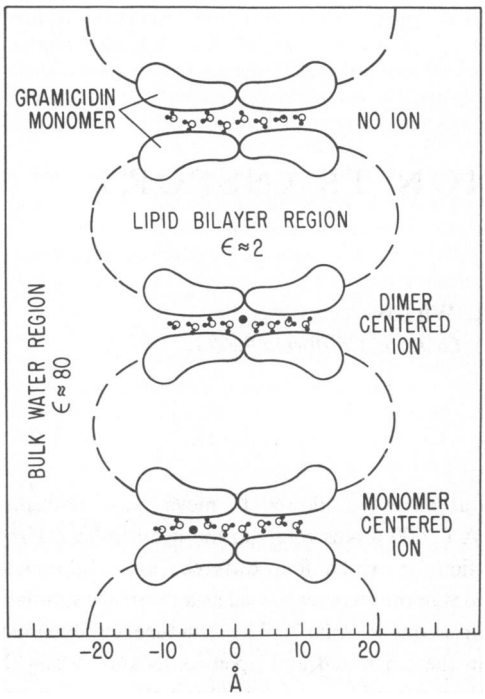

FIGURE 1 A highly schematic representation of gramicidin dimers (pear-shaped objects) embedded in a membrane (enclosed within dashed lines [---]) spanning interfaces to bulk water. Shown are representations of the three systems modeled in this study, an ion-free system (*top*), a dimer-centered ion system (*middle*), and a monomer-centered ion system (*bottom*). The open circles (○) represent oxygens of water molecules, while the larger filled circles (●) are ions. Although shown here, the bulk-water and lipid-bilayer regions are not included in the present calculations.

by Urry that suggests that the ion conducting unit is an unusual left-handed helix containing 6.3 peptide units per turn (17). This unorthodox structure is possible due to the presence of alternating D and L amino acids. Urry (17) points out that the hydrophilic polar peptide backbone of this structure lines the inside of the channel where it can interact with channel water and ions, while the largely hydrophobic amino acid residues dissolve into the surrounding hydrophobic interior of the lipid membrane.

As subsequent discussion will focus on the nature and magnitude of the barriers to ion transport through gramicidin, it is instructive to review various descriptions, both theoretical and experimental, of the energetics of ion transport. As a first approximation, the magnitude of the dielectric barrier can be approximated using the Born (18) ion self-energy model, $(ze)^2/2\epsilon r$. Thus, the difference in energy between a solvation sphere of radius (r) of 10 Å and a dielectric constant (ϵ) of 2 and the same size sphere but with ϵ of 81, with each surrounding an ion of radius 1 Å, valence (z) 1, and unit charge (e), is ~300 kJ/mol, or ~120 kT (where k is Boltzmann's constant and T the absolute temperature). A high dielectric channel through the membrane can significantly reduce this barrier as has been shown in several electrostatic calculations that use average dielectric contributions estimated for a polar channel interior (19–21). These calculations show that the existence of such a gramicidin-like channel can reduce the dielectric barrier to ~7–11 kT. Application of Erying rate theory to experimental conductances has led to derived activation free-energy barriers of ~20 kJ/mol or ~8 kT (2,22,23). Although the channel models are very approximate (several assumptions necessitated by the continuum models are made about the effective dielectric constant of the channel interior, which may be inexact in light of the carbonyl structure of the interior pore wall and the effects of linear water discussed later), the presence of a high dielectric channel provides at least a reasonable semiquantitative picture.

Models based on ion-induced shifts of the ^{13}C nuclear magnetic resonance spectra (24,25) and low resolution x-ray structures (13) suggest that an ion binding site exists close to the mouth of the pore and is the rate limiting barrier to transmembrane diffusion. These data have also been interpreted to show that any barrier at the center of the channel is smaller in comparison (25). The applicability of an Erying rate theory model for gramicidin has been questioned (26,27), and therefore it is of great interest to understand on a molecular level how the gramicidin system can so effectively reduce the large centrally symmetric dielectric barrier, which would exist in the absence of the channel.

Although debate continues on the predominate structure of gramicidin A in membranes (28,16), experiments strongly suggest that two gramicidin molecules dimerize head-to-head (i.e., formylated amino-end to formylated amino-end) to form a channel ~0.4 nm diameter and ~3 nm long (25,29). It is suggested that the left-handed helix lies in a shallow well in the potential surface such that it can rather easily distort (17,30,31), both in terms of helix conformation and in terms of the carbonyls being able to swing down from their original hydrogen-bonded positions in the helical cylinder of the peptide backbone in order to partially surround and solvate the ion, the negative oxygens of the carbonyls replacing some of the negative oxygens of water molecules that would be present for an ion solvated in bulk water. This carbonyl solvation is envisioned as occurring in a flexible manner that can accommodate a variety of small positive ions, the distortion of the helix following the ion as it moves within the channel, like a pig in a python.

Gramicidin is thus uniquely suited to a study of the underlying molecular basis for ion transport due to its simple and relatively well-defined structure and to the wealth of experimental data available for comparison with theoretical predictions. Several conformational studies investigating the local energy minima of the gramicidin structure in the channel have been reported (30–33). However, these studies allow only selected torsional degrees of freedom to vary and are performed in the absence of ions and waters. Two recent molecular

dynamics studies on a simplified gramicidin with ion model have been reported (34,35), but the simulations use several approximations, such as neglecting explicit waters, imposing a rigid hexagonal-like helix with librating carbonyl groups, and, in the earlier work, constraining the ion to move only along the channel axis.

We extend previous calculations of gramicidin by adding flexible geometry including all translational, rotational, and vibrational (stretches, bends, and torsions) degrees of freedom (36,37), room temperature dynamics, and the explicit inclusion of channel waters and four different ions. While the time scale of these initial calculations is too short to simulate an ion diffusing across the entire dimer, several features of ion solvation inside a peptide pore, both of a structural and dynamical nature, are observed in the model and discussed including (*a*) the structure of ion solvation in a water-filled gramicidin channel, (*b*) the extent of carbonyl bending as a function of ion type and location in the pore, (*c*) the energetics of ion solvation with respect to peptide and water structure, (*d*) the dynamic motions of the peptide, waters, and ions, and (*e*) the surprising role, at least in our model, of linear single-file arrays of oriented waters in narrow channels. Hopefully, studying ion solvation and transport in such a simple channel will also help the modeling and the understanding of these same processes in other more biologically significant systems.

METHODS

Molecular dynamics, the calculation of the classical time evolution of atomic trajectories, allows us to calculate the motions of gramicidin under various physical and chemical conditions. We have adapted a force field that describes the interactions of proteins, waters, and ions to run on an array processor (the Floating Point Systems AP-120B) thereby allowing significant calculations at a reasonable cost (38,39). The force field reflects a standard set of potential energy equations utilizing a Lennard-Jones 12-6 plus coulombic potential for nonbonded atom pairs and harmonic potentials for bond stretching and angle bending as well as a standard torsional potential. The model thus permits motion involving all nuclear degrees of freedom and includes all hydrogens explicitly. The functional form of the potential energy expression of the force field is

$$V = \sum_{\substack{\text{nonbonded}\\ \text{atom pairs}}} 4\epsilon_{ij}\left[\left(\frac{\sigma_{ij}}{r_{ij}}\right)^{12} - \left(\frac{\sigma_{ij}}{r_{ij}}\right)^{6}\right] + \frac{q_i q_j}{r_{ij}}$$
$$+ \frac{1}{2}\sum_{\substack{\text{bond}\\ \text{lengths}}} K_b(r - r_{eq})^2 + \frac{1}{2}\sum_{\substack{\text{bond}\\ \text{angles}}} K_\theta(\theta - \theta_{eq})^2 \qquad (1)$$
$$+ \frac{1}{2}\sum_{\substack{\text{torsion}\\ \text{angles}}} K_\phi(1 + \cos n\phi).$$

The first summation in this equation represents the nonbonded interactions using Lennard-Jones 12-6 plus coulombic potentials, where r_{ij} is the distance between atoms i and j, q_i and q_j are their electrostatic charges. For the Lennard-Jones interaction, ϵ_{ij} is the minimum energy and σ_{ij} the distance at zero energy. In addition to interactions between pairs of atoms on different molecules, nonbonded interactions are defined to include pairs of atoms within the same molecule if they are separated by more than two bonds. The second and third summations are simple harmonic potentials describing displacements from equilibrium values of bond lengths ($r - r_{eq}$) and bond angles ($\theta - \theta_{eq}$), respectively. The last summation over torsional angles, where ϕ is the torsional angle, provides torsional rigidity. The parameters K_b, K_θ, and K_ϕ are the force constants for bond stretching, bond angle bending, and torsional motion, respectively.

Parameters for the nonbonded peptide-peptide interactions were taken in part from work by Hagler et al. (40–44), where several types of experimental data are used to fit an empirical set of peptide parameters to the various potentials. We have included tables of the parameters used in the present calculations in the Appendix. The intermolecular water potential used is the single point charge (SPC) model of Berendsen et al.(45), which is essentially equivalent to the transferable intermolecular potential surface (TIPS) model of Jorgensen (46). The SPC potential was chosen because of the ease with which it can be combined with existing polypeptide and protein potentials. Because the peptide and water nonbonded interactions are both described by Lennard-Jones plus coulombic functions, the parameters describing protein-water interactions were easily approximated by applying a geometric mean combination rule (47) to the various peptide-water atom pair parameters. Appropriate Lennard-Jones parameters for ion-water and ion-peptide interactions were derived following Heinzinger and Vogel (48) by combining parameters for rare gases (representing the inner core of the ion) with the appropriate peptide or water cores (again using geometric mean combination rules) (47). The explicit parameters for all these interactions are given in Tables V and VI of the Appendix.

The intramolecular potentials (bond stretch, bend, and torsional rotation) for the peptides were adapted from a subset of preliminary valence force field parameters derived by Hagler and co-workers (see Tables VII, VIII, and IX in the Appendix). While the valence force field (37) includes cross terms between the various bonded interactions, the current version of the dynamics algorithm on the array processor did not provide for cross terms. As is a common practice, we have taken only the diagonal terms from this preliminary valence force field. The intramolecular potential for water was one derived from vibrational spectroscopy and departs from the expression in Eq. 1 in that it is anharmonic (49,50).

The time step of integration used during equilibration was 1.0×10^{-15} s. For the final data collection runs, a time step of 0.5×10^{-15} s was used. The integration is a version of the Verlet algorithm (51) with modifications by Andersen (52). No nonbonded cut-off distance was used, thus allowing every atom to interact with every other atom (requiring ~180,000 nonbonded calculations per integration step). On the array processor, the rate of calculation for the 600 atom system was 3.1 s/integration step, or 52 min of real time per picosecond of simulated time.

The molecular dynamics calculations were begun by using as a starting conformation the Urry head-to-head dimer model (17) with 6.3 residues per turn (a left-handed helix with [ϕ_L, ψ_L, ϕ_D, ψ_D] angles for the asymmetric dipeptide unit of [−144, 132, 104, −118] in degrees). From experimental evidence, this conformation is believed to be the appropriate one for the ion conducting unit in membranes (13, 25, 53–55). Recent energy minimization calculations also support this structure (33). This initial structure was then minimized in energy to relax any local strains in the geometry, which we found did not appreciably disturb the basic helix. Next, 13 waters were placed inside the channel and allowed to gradually equilibrate while the peptide atoms were kept fixed. Although initially placed entirely inside the pore, they soon repositioned themselves so that only eight or nine remained in single file in the pore, while the remaining waters formed small clusters at each end.

Following this initial minimization and equilibration, all atoms were allowed to move and the system was gradually heated by adding to the calculated accelerations a term proportional to the previous velocity until the temperature approximated 300 K (requiring a total of ~30 ps of simulation). After thus achieving an initial dynamic structure, further equilibration was carried out for ~20 ps at 300 K during which the system remained stable (operationally defined by the helical structure remaining

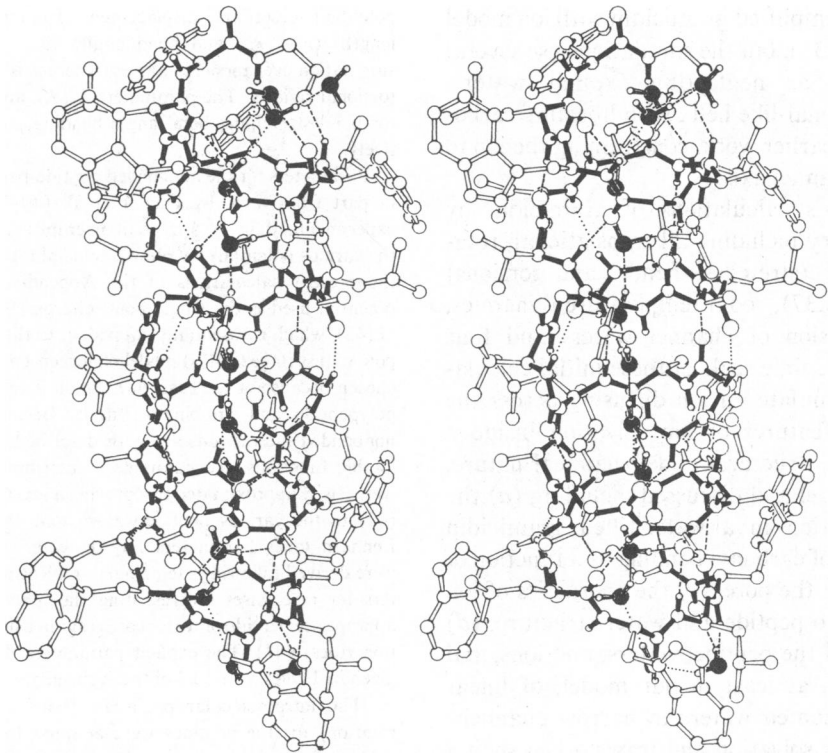

FIGURE 2 No ion. A stereo Oakridge Thermal Ellipsoid Plotting program (ORTEP) style model of the gramicidin-A dimer with only water inside the channel. Shown is an instantaneous conformation during a molecular dynamics simulation of the Urry head-to-head model at 300 K. The drawing also shows the hydrogen bonds (dotted and dashed lines) present at this instant. The peptide backbone and the water oxygens have been filled in (●) and the nonpolar hydrogens have been omitted for clarity in the illustration (but not in the dynamics). Note the conserved orientation of the water dipoles all pointing approximately in one direction.

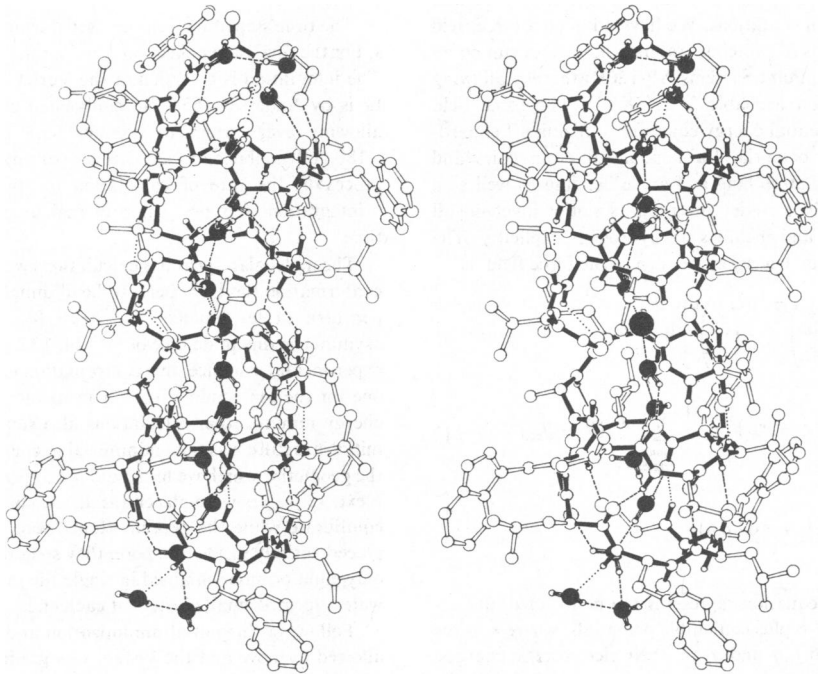

FIGURE 3 Dimer centered. An instantaneous picture of the ion plus water plus gramicidin-A system with a sodium ion placed in the center of the dimer. The ion is filled in (●) and enlarged for easy identification. Note again the conserved orientation of the water dipoles in opposite directions on either side of the ion so as to point their negative ends toward the positive ion.

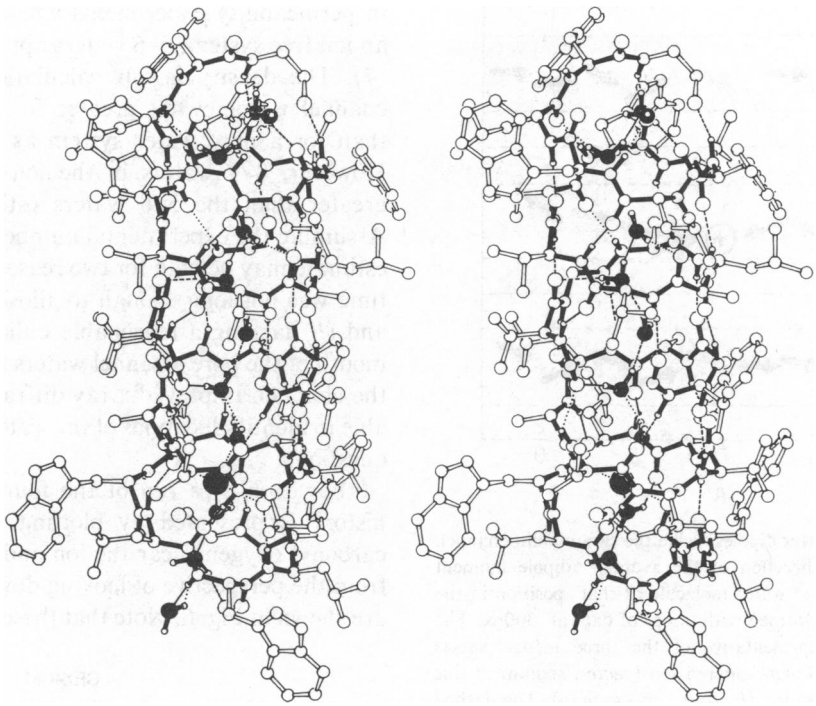

FIGURE 4 Monomer centered. An instantaneous picture of the ion plus water plus gramicidin-A system with a sodium ion placed in the center of one monomer. The ion is filled in (●) and enlarged for easy identification. Note the conserved orientation of the water dipoles in opposite directions on either side of the ion so as to point their negative ends towards the positive ion.

intact). It was observed during these equilibration runs that the water dipoles tended to hydrogen bond via one hydrogen to the peptide backbone and via the other to an adjacent water. The water oxygens always hydrogen bond to adjacent waters, and the dipoles of the single-file waters in the pore thus always point in the same general direction as seen in Fig. 5.

Following equilibration, a water molecule was replaced by a cesium ion. The charge of the cesium ion was turned on gradually (from 0 to 100% over 20 ps) to avoid sudden coulombic perturbations. At the beginning of this run, the peptide and waters were kept fixed while the ion found a suitable starting position, and then all the atoms were released to equilibrate. To sample different local channel environments without having to compute the diffusion of an ion across large distances (an important calculation but beyond the scope of this preliminary investigation), two of these runs were carried out with the ion replacing in each case different waters, one at the center of the dimer and one at the center of one of the monomers (see Figs. 1–5) In both cases, the waters with their oxygens oriented away from the ion were observed to quickly rotate to orient their negatively charged oxygens toward the ion (see Fig. 5). This occurred in a chainlike fashion and was complete in <1 ps, the closest water reorienting first followed by its neighboring water (the next closest) and so on until all the waters to that side of the ion had turned around. Again, short equilibration runs (5 ps) were made following each of the ion placement runs. Although there were significant deviations from the initial pore structure due to the presence of the ion, in all cases the overall helix remained intact on our time scale. At this point, the cesium ion was successively replaced with progressively smaller ions in order to prepare similar models with different ions. In each case, the models were equilibrated for several picoseconds until the system had been able to adjust to the new ion before making the next substitution.

To insure that the kinetic energy of the system was evenly distributed among all the atoms at the temperature of interest, we employed a velocity randomization algorithm that randomly assigned velocities consistent with a Maxwell-Boltzmann energy distribution for that temperature. This velocity randomization was applied six times for each system, each application separated by 100 steps of dynamics, as a final step in the equilibration process.

Thus, we have nine different model systems: one without an ion, and two each (ion centered in monomer and ion centered in dimer) for each of the four cations tested: lithium, sodium, potassium, and cesium. After equilibration, each of these systems was run for 5 ps, the trajectories of each run provided the data for analysis.

In addition to the dynamics trajectories, structural minimizations were conducted to investigate the nature of various local minima. Configurations were sampled at 1-ps intervals during the dynamics runs for subsequent energy minimization. Alternate sets of 100 steepest descent and 100 dynamics iterations were used to minimize the energy of each configuration until a set of steepest descent iterations failed to produce an energy more than 0.01% lower. Minimization by this criteria required 10–15 sets of both steepest descent and dynamics iterations for each system.

RESULTS

Because of the enormous volume of data inherent in molecular dynamics simulations, we present the results in a pictorial manner and point to obvious structural and dynamic features significant in understanding ion transport in gramicidin A. Although it is our goal to calculate further properties that can be compared directly with experiment, such calculations are extremely demanding computationally and will be published in a subsequent paper.

The number of single-file waters observed here agrees roughly with the experimentally determined number of 7–9 for channels singly occupied with ions (8,9). However,

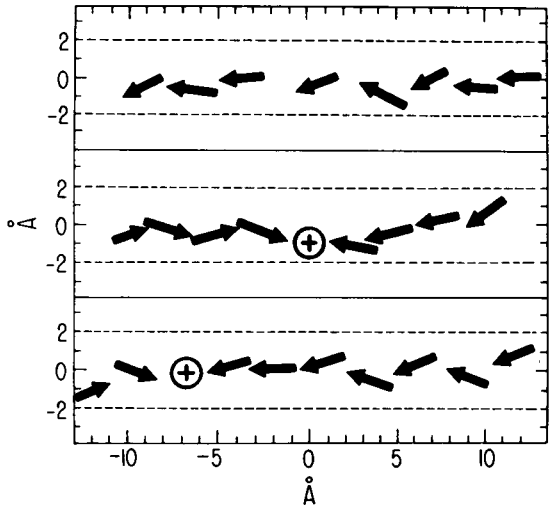

FIGURE 5 Orientation of water dipoles inside the gramicidin channel. Each arrow represents the direction of the average dipole moment (magnitude is arbitrary) of the water molecule at that position in the channel. The average was performed with 0.5 ps of data at 300 K. The three systems shown are representative of the three model classes investigated, ion-free (*top*), dimer-centered ion (*center*, sodium in this figure), and monomer-centered ion (*bottom*, also sodium). The dashed lines (---) show approximately where the surface of the interior channel atoms begin.

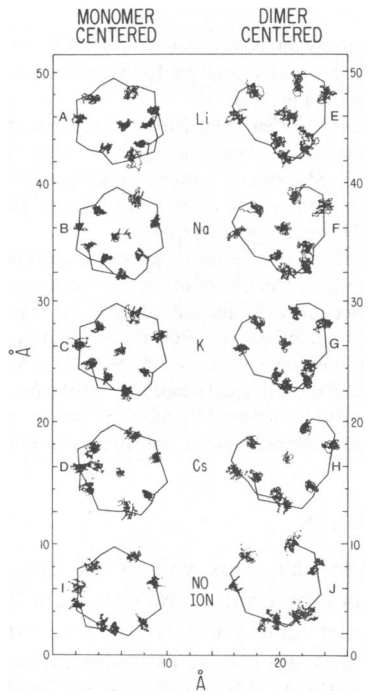

FIGURE 6 Trajectory plots of the eight closest peptide units surrounding the ion for the nine simulations viewed from the end-on perspective, i.e., looking down the pore. *A–D* correspond to ions in the monomer-centered postion, while *E–H* correspond to the dimer-centered ions. *I* and *J* are of the monomer-centered and dimer-centered regions but in the absence of any ion. The dense globular lines correspond to the actual time trajectories of the ion (in the center) and carbonyl oxygen over 5 ps. A stick drawing of the average backbone position for the eight closest peptide units is superimposed as a reference.

in permeability experiments where the conditions reflect an ion free system, 5–6 waters appear to be in the channel (7). The density in our calculation of water inside the channel is somewhat greater for an ion-bearing system than for a pure water system as can be seen in Fig. 5. However, 8–9 waters in the ion-free simulation is still greater than the 5–6 waters estimated experimentally. Assuming the experimental number is real, our pure water estimate may be high for two reasons: (*a*) the equilibration time was not long enough to allow the waters to leak out and (*b*) lacking a reasonable bulk-water interface at the mouth of the pore, channel waters may prefer to remain in the channel. Improved x-ray diffraction analysis might be able to identify locations of the waters and help resolve this question.

For each 5-ps run of the four ions, an average time history is presented by plotting the trajectories of the carbonyl oxygens near the ion and of the ion atom center from the perspective of looking down the pore. These plots are shown in Fig. 6. Note that these trajectories correspond

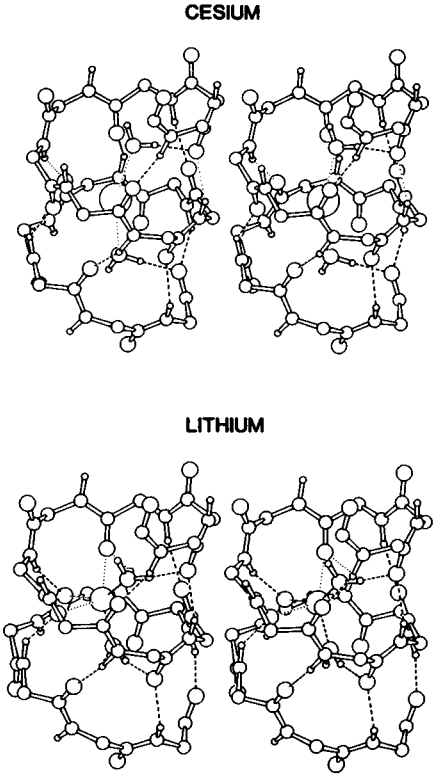

FIGURE 7 Minimized ion-peptide-water structures. Stereo ORTEP drawing of the peptide backbone, ion, and two adjacent waters in two monomer-centered systems, lithium and cesium. The structures shown are energy minimized from the final dynamic configuration and displayed with the pore axis vertical. The cesium ion has been enlarged for easy identification. The carbonyl structure is seen to be highly distorted by the lithium ion while remaining relatively unperturbed in the cesium case. Also, the waters around the lithium show a clear bridging structure as they coordinate both to the ion and to carbonyls across from the ion. The bridging structure is less pronounced around the cesium. The dashed lines (---) represent interatomic distances of <2.5 Å to the lithium ion and 3.0 Å to the cesium ion.

to the volume sampled by the atom centers and do not represent the atomic volume itself. For reference, the average position of the peptide backbone during the simulation is superimposed onto the atom trajectories and trajectory plots for a pure water (ion-free) system are provided as well. A more detailed, minimized structure for two interesting cases (monomer-centered lithium and cesium) are shown in Fig. 7.

An important feature recognized early for the Urry gramicidin model (17) is the ability of the carbonyl groups to bend into the pore to help solvate the ion. This property is measured in our model calculations by computing the angle between the carbon-oxygen vector and the pore axis. To minimize the effect of axis fluctuations, the pore axis is dynamically defined for each configuration as the line connecting the centers of the six outermost alpha carbons at either end of the dimer. While this definition assumes that the channel is linear when, in fact, the structure on average in our runs is slightly banana shaped (by ~5°), it does serve as a consistent reference. This time average of the angle of deflection for a carbonyl bond is defined as Ψ. A negative angle indicates that the carbonyl group bends toward the center of the pore.

Fig. 8 shows Ψ for all 32 carbonyl groups for each of the 8 ion systems as a function of carbonyl carbon location along the pore. To emphasize the perturbations caused by

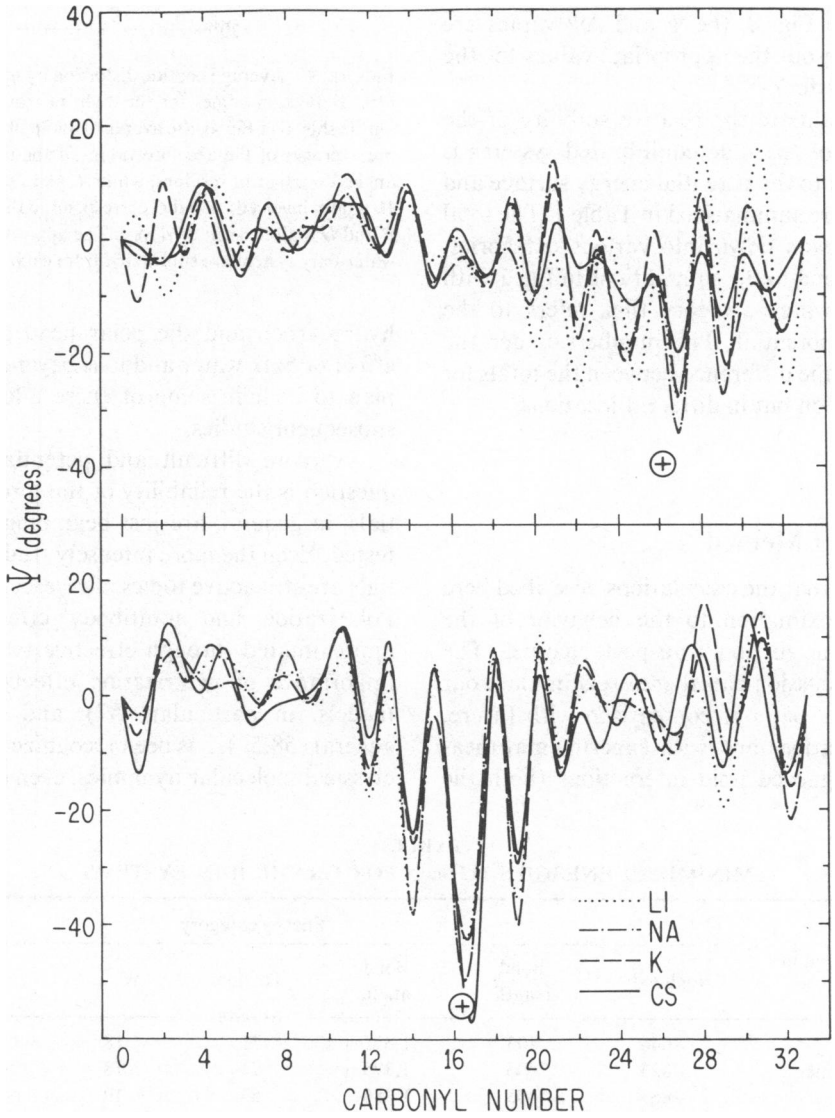

FIGURE 8 Ion-induced peptide distortion. The angle Ψ represents the ensemble average of the angles formed by the carbonyl bond and the channel axis. The corresponding Ψ from a water-only reference system is subtracted from the Ψ for an ion-plus water system to emphasize perturbations caused by the ion. The resultant Ψ is then graphed as a function of the carbonyl number for both monomer-centered ions (*upper* graph) and the dimer-centered ions (the *lower* graph). A negative angle corresponds to deflection toward the pore axis. The ⊕ symbols identify the approximate location of the ion during the simualtion. The marked sinusoidal fluctuations of Ψ around the ion is due to the coupling of adjacent carbonyls (the inward deflection of a carbonyl toward the ion being balanced by an outward deflection of its neighbors) and helps to preserve the overall helical conformation even in the presence of local ion-induced distortion.

the ion, reference carbonyl deflections in the water-only (ion-free) simulation have been subtracted from those for each of the ion models. Each curve represents a time average over 1,000 configurations collected at 0.005-ps intervals for a total of 5.0 ps. The standard deviations of the angles are approximately ±10°C.

The overall effect of ion type and position on the peptide as measured by carbonyl distortion is summarized in Fig. 9. In Fig. 9 *A* and *B*, $\Delta\Psi$, the absolute value of the difference between carbonyl angles on adjacent residues, is averaged and graphed for the eight carbonyl groups surrounding the ion. The average Ψ for these eight carbonyls is shown in Fig. 9 *C* and *D*. Figs. 9 *A* and *C* correspond to the ion being centered in the monomer, as shown in Fig. 4, while Figs. 9 *B* and *D* correspond to dimer-centered ions, as shown in Fig. 3. As in Fig. 8, the Ψ and $\Delta\Psi$ values are adjusted by subtracting out the appropriate values for the reference water-only system.

To quantitatively estimate the relative stability of the various systems, each of the nine equilibrated systems is minimized with respect to the potential energy surface and the resultant energies are summarized in Table I. The total potential energy is broken down into various categories. The categories correspond to the summations in Eq. 1 with the exception of the water category that refers to the intramolecular water potential. The numbers under the difference heading are the difference between the totals for systems with the same ion but in different locations.

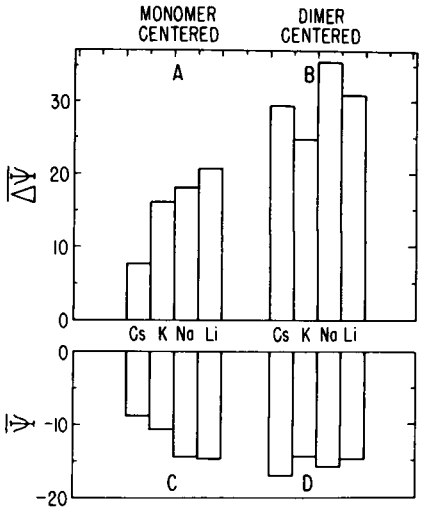

FIGURE 9 Average peptide distortion by monomer- and dimer-centered ions. Deflection angles for the eight nearby carbonyls surrounding the ion, as shown in Fig. 6, are averaged and plotted for each system. *A* and *B* are averages of the absolute value of the differences between carbonyl angles on adjacent residues, while *C* and *D* show the mean angle for the 10 angles involved. *A* and *C* correspond to the monomer-centered ion and *B* and *D* to dimer-centered ions. The appropriate reference values of the water-only system are subtracted from each system before averaging.

DISCUSSION

Limitations of Method

It must be emphasized that the calculations described here are only a first approximation to the behavior of the gramicidin A system as an ion transport channel. The present speculative discussion can therefore stimulate our thinking and serve as a basis of comparison with future, more ambitious calculations and with experimental measurements. We have ignored lipid interactions (both the hydrocarbon and the polar head groups) as well as the effect of bulk water and ions beyond the pore opening. We plan to include some of these additional components in subsequent studies.

A more difficult and potentially more troublesome question is the reliability of the force field. Peptide potentials, in general, are just beginning to be understood and tested. Even the more intensely studied water-water potentials are still active topics of research and controversy (56). Polarization and multibody effects are only crudely approximated through effective two-body potentials. The importance of polarization effects in both ion transfer models, in particular (57), and biological systems, in general (58,59), has been recognized and discussed. Lastly, classical molecular dynamics, even on the correct potential

TABLE I
MINIMIZED ENERGIES (kJ/mol) FOR GRAMICIDIN SYSTEMS

Ion	Centered in	Energy category						
		Nonbond	Bond length	Bond angle	Torsion	Water	Total	Difference
No ion	—	−646	403	1,375	71	18	1,221	—
Cesium	monomer	−823	405	1,375	71	18	1,046	44
	dimer	−869	405	1,380	67	19	1,002	
Potassium	monomer	−911	405	1,379	72	21	966	4
	dimer	−907	403	1,380	66	20	962	
Sodium	monomer	−985	402	1,376	70	21	884	0
	dimer	−987	403	1,378	67	23	884	
Lithium	monomer	−1,028	401	1,377	69	23	842	−1
	dimer	−1,031	403	1,380	69	22	843	
Average deviation		±10	±1	±4	±4	±1	±15	—

surface, is still only approximations of the inherent quantum dynamics of molecules (60–62).

In spite of these limitations, there are undeniably intriguing processes occurring in even this simplified model. We speculate here about several features of ion transport that have been observed in the calculations. It is the purpose of this discussion to enlarge the scope of conceptualization about the ion transport mechanism and to encourage both more elaborate and hopefully more accurate calculations and more debate concerning the details of this model as well as experimental tests. While our discussion is pertinent to the simulated model, the relevance of our model to molecular reality is as of yet unconfirmed.

General Structural Features

Although the present calculations are designed to investigate the dependencies on ion type and location, there are several structural features generally present regardless of the ion or its position. One of the most striking is the overall organization of the water molecules inside the channel.

The hydrogen-bonded network can be examined in Figs. 2–4 and shows that, in general, each water bonds one hydrogen to an adjacent water and the other hydrogen to a nearby carbonyl oxygen. Note that the hydrogen bonds between carbonyl and amide groups within the peptide are still present and, in fact, except where an ion is close by, the geometry of the intra-peptide hydrogen bonds is relatively undisturbed by the presence of the extra hydrogen bond to the water. Furthermore, because hydrogen bonds are relatively weak (~16 kJ/mol), they are continuously forming and breaking and at any given instant and may be momentarily too long to meet the dotted line drawing criteria in Figs. 2–4 (operationally defined as a hydrogen-oxygen nonbonded distance of <2.2 Å). That the water dipoles remain aligned over a distance of ~25 Å throughout the simulation is distinctly different from the much more random orientations observed in bulk water. The unusual linear chain structure of the interior waters raises interesting questions about the special properties of linear water, which are discussed in more detail in later sections.

The participation of solvating carbonyl groups embedded in the pore wall has been used to explain the mechanism of ion transport in gramicidin (1). We have observed that the coordination of carbonyl oxygens with ions is also a general structural feature and have summarized the data in Fig. 9. A detailed picture of the carbonyl bending is given in Fig. 8, where the average angle of deflection out of the pore wall for each of the carbonyl groups in the eight systems is graphed as a function of carbonyl location along the peptide backbone. The perturbation can be seen in Fig. 8 to be relatively local, distorting every other carbonyl (~6) near (~2 turns of the helix) the ion, regardless of the ion type or location. Because carbonyl dipoles on adjacent residues point in opposite directions in gramicidin ("point" in this context refers to the predominant orientation, either parallel to or antiparallel to the pore axis), those carbonyl oxygens closest to the ion will be flanked by carbonyl oxygens pointing away from the ion, even though the carbonyl carbons are essentially equidistant from the ion. In tilting toward an ion from their positions embedded in the pore, carbonyls pointing toward the ion have more to gain in terms of energy stabilization than do adjacent carbonyls pointing away. To appreciate the impact this difference makes, calculations of various carbonyl-ion geometries show that for carbonyl groups pointing toward the ion, a rotation away from the pore wall by ~30° (which is typical for carbonyls near an ion) can decrease the electrostatic energy of interaction with the ion by 16–30 kJ/mol (depending on the ion type) with respect to an orientation embedded in the pore wall. A similar rotation of an adjacent carbonyl (one whose carbon is the same distance from the ion but whose oxygen is pointing away from the ion) can achieve only a 8–10 kJ/mol decrease. This appears to be insufficient to deflect these carbonyl oxygens and strong deflection is therefore only observed for every other carbonyl. The bending of carbonyl groups, which we observe, is also consistent with previous analyses of the energy surface of gramicidin that have suggested that the backbone lies in an easily distorted region of the Ramachandran map (30).

Structure as a Function of Ion Type and Location

In the eight ion-containing systems simulated, two major structural features are found to be strongly dependent on ion type and location: (*a*) the degree of carbonyl and backbone distortion, and (*b*) the displacement of the ion from the pore axis.

Monomer-centered Ions. For ions located at the center of a monomer as in Figs. 4 and 7, the deflection of the carbonyl groups into the pore is found to be strongly dependent on the ion considered. Figs. 9 *A* and *C* show that the distortion is greatest for lithium and least for cesium whether one takes the average angle for the eight surrounding carbonyls (Fig. 9 *A*) or a difference between adjacent carbonyls (Fig. 9 *C*). Also, the smaller ions, lithium and sodium, in the monomer-centered systems are displaced away from the central axis of the channel, as can be seen clearly in Figs. 6 *A* and *B*. More subtle structural features are shown in Fig. 7, which compares the local minimized water-peptide structure about the cesium and lithium ion. The smaller ion (lithium in Fig. 7) is solvated from one side of the channel axis by its two nearest neighbor waters, which act as bridges to nearby carbonyls, and from the other side of the channel axis by three distorted carbonyls. As one progresses to larger ions, e. g., cesium, the ion is observed to be more centered on the channel axis, essentially equidistant from all surrounding carbonyls, and the adjacent waters move further apart and more in line axially with the ion. Potassium and especially

cesium appear to be large enough to deflect equally each of the carbonyls in their vicinity as can be seen in Figs. 6 *C* and *D*. In fact, the level of distortion in the cesium case (Fig. 6 *D*) is practically indistinguishable from the pure water case (Fig. 6 *I*).

Both of these structural features suggest interesting mechanistic models. For example, because small ions tend both to be displaced away from the pore axis and strongly deflect the carbonyl oxygens into the pore, the electrostatic attractiveness of the oxygens is more pronounced than for larger ions that do not deflect the carbonyls strongly and remain further away. For the minimized orientations in Fig. 7, this accounts for a 70 kJ/mol difference between the most favorable carbonyl-ion interactions in the cesium and lithium cases. The smaller ions may therefore experience a larger frictional force as an impediment to diffusion directly as a result of stronger interaction with the channel wall.

Furthermore, because of this attraction to the pore wall, the smaller ion may be prefer to roll along the helical backbone or jump across the pore to a new site on the opposite side of the channel. Either of these scenarios would require the ion to travel a longer distance than the path of a larger ion, which can span the pore diameter. For example, if an ion is displaced 1 Å from the center of the gramicidin helix and constrained to follow a helical path parallel to that of the channel helix, it will travel 1.7 times further than an ion traveling straight down the center. Since the time varies as the square of the distance, this means the ion will take three times as long to diffuse across the channel and its measured diffusion coefficient and conductivity would be one-third as great, all other things equal. The experimental conductance ratios among lithium, sodium, potassium, and cesium are ~0.29:1.0:1.8:2.9, respectively (2). Thus, such a mechanism could easily account for the ratio between sodium and cesium. Of course, such effects could be negligible if random diffusion were not the rate-limiting process in the ion-transport process. However, given that ions pass through gramicidin easily (2), such a diffusional mechanism may be important.

Dimer-centered Ions. The average bending of carbonyl groups is found to be much more pronounced where the two monomers join head-to-head (and the covalent linkage along the helix is broken) than in the center of one monomer. Comparison of Fig. 9 *A* and *B* shows that the average carbonyl distortion at the dimer's center is 1.5–3 times greater for a given ion than in the monomer-centered case. However, the strong dependence on ion type observed for the monomer-centered cases is absent in the dimer-centered ions. Moreover, the ions tend to remain close to the pore axis even for the smaller ions, as can be seen in Fig. 6 *E–H*. However, the overall distortion of the peptide is noticeably greater, presumably because the loose ends of the peptide are more flexible and can adapt freely to the most optimal carbonyl-ion orientation. The channel cross section of the dimer-centered ion models changes shape significantly from lithium to cesium as can be seen in the end views of Fig. 6. The channel center seems to expand gradually as the ion size increases, producing a flattened cylinder until, as seen in Fig. 8 for the case of dimer-centered cesium, the formyl carbonyl groups (numbers 16 and 17) are bent almost 60° away from the channel wall and are pushed back and away from each other.

The peptide's increased flexibility at the channel center due to the dimer junction suggests a mechanism for lowering the free energy at the center of the channel. As discussed above, the simulations show (see Figs. 2–4, 6, and 8) that the pore seems to be more flexible at the center, the carbonyls bending dramatically toward the ion at the apparent expense of helical distortion. Such increased flexibility is obviously partly due to the break in covalent bonding at the dimer junction and possibly also due to the particular (generally smaller) amino-acid side chains at the formyl ends.

To help to quantitatively understand the role of flexibility, five configurations are selected at regular intervals during the five ps of dynamics and energy minimized. Table I provides a quantitative estimate of the minimized energy broken down into several categories. The deviations given in Table I are the average deviations from the mean value for the five minimizations and are approximately the same for all the systems. The major source of deviation is the convergence to different local minima from the different starting configurations. The pattern of energy distribution among the various modes (nonbond, torsion, etc.) and relative to the ion type and location is complex, and the results from these minimizations can provide only a partial picture. For example, minimized energies (where the temperature is essentially 0 K) do not necessarily reflect the same patterns as among average room-temperature energies. Also, because bulk-water interfaces are not present, the nonbond contribution for monomer-centered ions is probably underestimated. Nonetheless, some statistically valid patterns are present.

The data in Table I support the idea of increased flexibility at the channel center. Although the distortion of the hexagonal cross section shown in Fig. 6 *E–H* is dramatic, Table I shows that the gramicidin structural energy (defined by the sum of bond length, bond angle, and torsional columns) varies little between monomer-centered and dimer-centered models, implying that distortion at the channel center is essentially costless in terms of energy.

There is experimental evidence as well that structural details of the channel center may be critical to the transport mechanism. Chemically linked dimers of gramicidin A (63) show a marked conductance decrease that could be explained qualitatively by the increased constraint imposed on the center of the channel by the covalent linking of the formyl head groups. Also, recent experiments where glycine is substituted for amino acids at the center of the

gramicidin channel (O. S. Andersen, personal communication) result in lower ion conductance.

Perhaps the most striking feature of Table I is the greater stability of the dimer-centered cesium compared with the monomer-centered cesium system. This is in marked contrast to the situation for the other ions where there is little, if any, statistically significant difference for monomer vs. dimer-centered placement of the ions. The greater stability for dimer-centered cesium can be directly attributed to more favorable nonbond interactions (accounting for 46 of the net 44 kJ/mol difference) and supports the idea that greater peptide flexibility at the channel center allows more optimal coordination of the ion with surrounding carbonyls. This effect is most prominent for cesium due to its size. Carbonyl groups cannot bend in toward a monomer-centered cesium since the ion is just about the right size to span the diameter of the channel. Therefore, when the more flexible carbonyls at the channel center are able to orient almost perpendicular to the channel axis (60°), the net effect is very pronounced. For the smaller ions, some carbonyl bending can occur at the monomer center so that the difference when compared with dimer-centered ions is small.

The fact that, with the notable exception of cesium, the energy of the channel with waters and ion does not vary significantly with the ion at two very different locations suggests that any models requiring free-energy barriers and/or wells should not depend heavily on structural features of the gramicidin peptide or channel waters to provide such barriers (or wells). Work currently in progress extending these calculations to free energy for ions at other locations and with a better bulk-water model will hopefully help clarify the microscopic basis for ion conduction.

Water Structure and Properties

As can be seen in Fig. 2, the inner most waters for the water-only channel have roughly parallel dipoles, all pointed in approximately the same direction. Whenever an ion is present (as seen in Figs. 3 and 4), the waters on either side reorient to point their oxygens toward the ion, even if the ion is on the opposite side of the pore. Fig. 5 shows the average (over 0.5 ps) orientation of the water dipoles inside the pore for three sample systems: (*a*) pure water, (*b*) dimer-centered sodium ion, and (*c*) monomer-centered sodium ion. The special properties of hydrogen-bonded chains have been recognized (64) and the presence of a highly conserved linear array of waters leads to several interesting phenomena in gramicidin.

Water-Ion Energetics. Although gramicidin A is usually thought of as an ion channel, the unique properties of the single-file array of waters suggest that the interior channel waters may be just as influential in solvating and transporting the ion as the peptide-lining of the channel. The primary utility of a peptide-lined cylinder then may be one of a suitable environment for forming and holding a linear array of waters rather than just an ion and should be thought of first as a water channel. This perspective has been suggested strongly by the following observations.

Electrostatic forces favor the specific orientation of water dipoles in the channel both with respect to neighboring waters and to the ion. We have found with the model we have used that such effects are very long range, the orientation of waters persisting across the whole pore (see Figs. 2–5). In fact, water-water (approximately dipole-dipole) interactions compensate for much of the solvation energy the ion loses from shedding its hydration shells as it enters the channel. To illustrate the solvation energy available in a pore of constrained linear waters relative to free cluster waters with no pore, the average potential energy for combinations of various ions with linear waters inside the pore (but excluding contributions to the energy made by pore atoms) is calculated during the simulations and compared with similar calculations on small water-ion clusters. Fig. 10 illustrates a typical configuration for these two systems. For the energy calculation of the pore ion-waters, four groupings are made, each including the ion with its two, four, six, and eight closest neighbor interior waters. In Table II, the average energy change observed by incrementally adding pairs of waters into the molecular dynamics calculation is tabulated for both the linear and the cluster system.

As the third and fourth waters are added, the average potential energy decreases more in the cluster than in the linear system, presumably because in one-dimensional

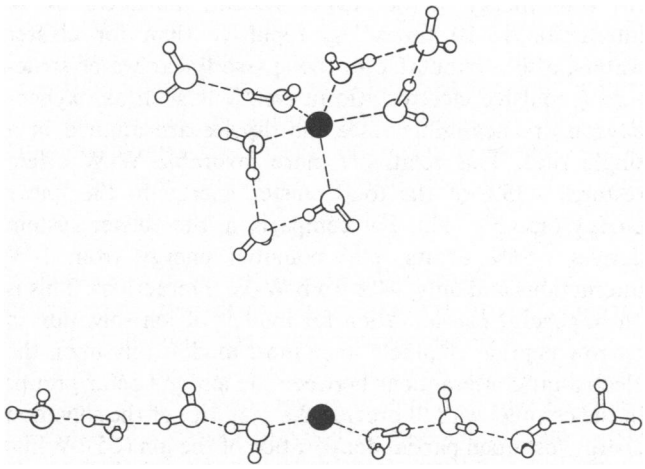

FIGURE 10 Instantaneous picture of the cluster (*top*) and linear (*bottom*) water-ion structures used to evaluate the relative contributions of ion-water and water-water interactions in the cluster vs. linear systems, which gives rise to both stronger oxygen-ion attractions and oxygen-oxygen and hydrogen-hydrogen repulsions. The linear system, while not having as strong attractive forces, has far smaller repulsive interactions, which results is an average solvation energy ~ 80° that of the cluster system.

TABLE II
CHANGE IN ENERGY (kJ/mol) FOR THE REACTION: $M^+(H_2O)_{n+2} \leftarrow M^+(H_2O)_n + 2H_2O$

$n, n+2$	Cluster				Linear			
	Li	Na	K	Cs	Li	Na	K	Cs
2,4	168	152	103	99	104	104	94	90
4,6	101	85	108	74	80	77	77	75
6,8	81	83	64	94	65	64	60	56
2,8	350	320	275	267	249	245	231	221

water they are forced to occupy the second hydration shell, while in the three-dimensional water cluster they can still coordinate from within the first hydration shell. The difference between linear and cluster systems is not as great for the addition of the fifth and sixth waters and for the addition of the seventh and eighth waters, even though the linear water pairs are now in the third and fourth hydration shell, while the cluster waters are never beyond the second shell. In the linear system, the seventh and eighth waters are 9 to 10 Å away from the ion and yet are contributing 60–95% of the incremental solvation energy of the seventh and eighth cluster waters, depending on the ion being solvated. Overall, the linear water structure can account for 71–84% of the potential energy of an equivalent cluster, even though on the average the cluster waters are much closer to the ion.

Detailed analysis reveals the source of the increased solvation capacity of a linear structure. By separating the potential energy contribution into two pieces, one arising from ion-water (I-W) interactions and the other from water-water (W-W) interactions, we find that, while the linear system's more distant waters recover only ~50% of the I-W energy of the cluster system, the linear W-W interaction is 10 times less repulsive than for cluster waters, also attributable to the sparse linear water structure (repulsive electrostatic interactions such as oxygen-oxygen are negligible since the dipoles are aligned in a single file). This relatively more favorable W-W effect restores ~35% of the total cluster energy to the linear energy (see Fig. 11). For comparison, the cluster system derives ~96% of its total potential energy from I-W interactions and only ~4% from W-W interactions. This is an important consideration for models of ion solvation in narrow peptide channels since most models rely upon the electrostatic interactions between the ion and polar groups in the channel wall to provide the majority of the solvation energy lost upon partial dehydration of the ion (65). While carbonyl solvation of ions is important, an equally important contribution may be the relatively more stable interactions among the waters remaining in the pore. Again, in our model, ~50% of the I-W energy of the innermost eight waters is lost as the ion goes from a cluster to a linear configuration. This is expected as the average water-ion distance has approximately doubled. However, ~35% of the energy is immediately recovered due to relatively more

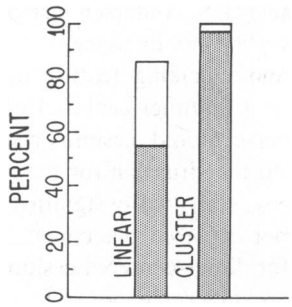

FIGURE 11 Analysis of the average water-water and ion-water energy contribution of linear and cluster ion-water systems containing one ion and eight waters. The shaded portion represents the ion-water contribution and the unshaded, the water-water contribution. The linear system consisted of four waters on either side of the ion constrained within the gramicidin channel. Both systems represent the average over the four ions tested, Li, Na, K, and Cs. The cluster system energy is defined as 100%.

attractive W-W interactions in the linear configuration. The ion-peptide interactions, thus, need only replace part, perhaps less than commonly estimated, of the solvation energy lost during dehydration of the ion. Perhaps the major role of the gramicidin pore should be one of providing a suitable electrostatic environment for the waters and of ordering the waters (an entropic contribution) into a linear array. Of course, to quantitate the entropic contribution, free energies must be calculated for a more realistic system with an ion solvated in a channel spanning bulk-water interfaces. However, these preliminary results do suggest that the contribution toward ion solvation of a linear arrangement of channel waters may be comparable with or perhaps even greater than that of channel wall solvation.

Water-Ion Correlations. Complementing the unusual energetics of linear water-ion interactions are the interesting correlations among the water and ion motions. As an example of a short-range correlation, Fig. 12 shows the two waters adjacent to the ion (1 and 3) to be highly correlated to the more rapidly oscillating ion motions, while waters further removed vary much more smoothly. Translational correlation among the water molecules is also long range, extending across the entire pore. In two cases during the simulation, an ion made short jumps of ~1 Å along the length of the channel. These jumps are accompanied by an almost simultaneous shift of all the waters in the pore in the same direction as the ion movement. Fig. 12 graphs the time history of the monomer-centered sodium system during a jump that lasts ~2 ps. It is clear from Fig. 12 that correlations in direction of motion extend well beyond adjacent molecules. Indeed, a shift of ~1 Å occurs at 1.0–1.6 ps for all molecules in the channel, seeming to begin with the waters furthest from the ion (upper part of the graph) and smoothly followed by the ion with its adjacent waters some 0.2 ps later.

This process is suggestive of a transient packing defect

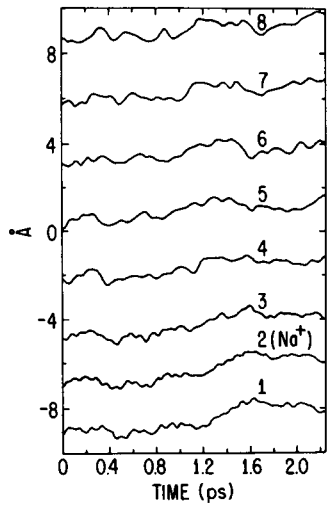

FIGURE 12 Translational correlations of water and ion. The translation movement along the pore axis of the channel water oxygens and a sodium ion is plotted as a function of time to show the high degree of correlation among the waters and ion. Note that motions between adjacent molecules and even across the entire length of the channel are well correlated. In particular, the upper four waters, numbers *5–8*, experience a concerted shift of ~1 Å in the positive direction at ~1.0 ps. This displacement is transferred within 0.2 ps to the ion and water at the other end of the channel (numbers *1–3*). Note also that the two waters adjacent to the ion (*1* and *3*) are highly coupled to the rapidly oscillating ion motions, while waters further removed vary much more smoothly.

mechanism first suggested in dense phase computer simulations by Rahman (66) where atoms are driven into small transient cavities by collisions from the side opposite the cavity. Also, since net ion movement seems to depend on concerted displacements of the entire channel of waters, a gating description similar to that described by McCammon (67) may also be appropriate. However, it is difficult from Fig. 12 to assign causality, i.e., which motions are forming cavities and which are filling them. Furthermore, because hydrogen bonds between waters are much stronger than typical van der Waals forces between atoms, waters may be pulled into a transient cavity as well as pushed by neighboring collisions. Any cavities that may be forming are so small and are filled so quickly (broken water-water hydrogen bonds, defined as oxygen-hydrogen nonbond lengths >2.2 Å, appear only occasionally between water molecules and are short lived, the hydrogen bond reforming within 0.5 ps), a more thorough analysis of the trajectories is required, which should also include peptide correlations, particularly those of the carbonyl groups, in order to determine the relative significance of such mechanisms.

Rotational correlations are also prevalent in these simulations. With the general constraint that the dipoles of the eight interior waters remain approximately parallel, waters in the channel in the absence of an ion rotate quite freely. Under certain conditions, it is observed that spontaneous flipping of the water dipoles does occur. During the water-only simulation, two waters at the end of the channel rotated to orient their dipoles in the opposite direction. This event is represented in Fig. 13 where the projection of the water-dipole moments onto the pore axis is plotted for the involved waters as a function of time. The order of events is clear. First, the dipole of the outermost (number 1) water (bottom of the graph) begins to rotate. Within 0.1 ps, the adjacent water begins a correlated rotation. The third water is further out of phase and affected to a lesser extent, while the fourth water remains essentially undisturbed. Approximately 1.5–3.0 ps after the waters begin their rotation, they return to the initial orientation. This was an isolated event that occurred with waters close to the pore opening where there are several randomly oriented waters close to the entrance that may help stabilize the reorientation. Furthermore, as can be seen in Fig. 13, the waters quickly reorient in <4 ps to their original orientation. Although the rotational correlation observed during this event spans at least three waters, it appears that there is a significant resistance to the reorientation continuing across the entire channel. Statistically, of course, it is only a matter of time before the entire chain of waters would flip, although our calculations are too short to measure the time.

The correlation of the water dipoles during this event is illustrative of the typical correlations observed. However, the water structure for the ion systems is more conserved

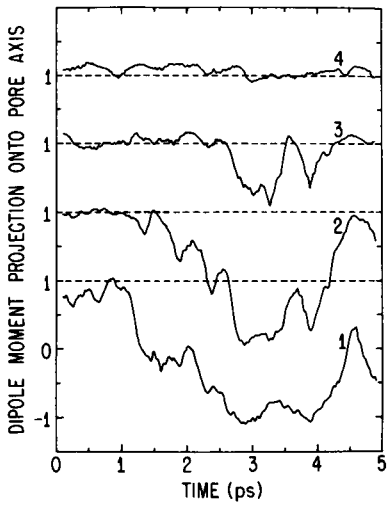

FIGURE 13 Rotational correlation of waters. The dipole moment (arbitrary units) is projected onto the pore axis for four waters in a water plus gramicidin system (no ion) and plotted as a function of time. The sign of the dipole indicates the overall orientation of the dipole, a zero value indicating a dipole oriented perpendicular to the pore axis and a typical value being 1. A relatively rare event is depicted here where the number *1* water (the outermost water at one end still considered to be in the channel) rotates to orient its dipole in the opposite direction. The subsequent rotation of the adjacent two waters, numbers *2* and *3*, shows the highly correlated orientational interactions. That there is a small barrier to dipole reorientation is qualitatively suggested by the central two waters, numbers *2* and *3*, returning to their original orientations after a few picoseconds. The dipole time history for each water is smoothed and displaced from the adjacent water for clarity, the dashed lines (---) providing reference values.

and no spontaneous flips were observed, the waters being strongly oriented by the presence of a positive charge in the channel.

The presence of strongly oriented dipoles in the channel interior suggests several interesting scenarios for ion transport. For example, as an ion completes its traversal of the pore, say from left to right, it leaves behind a column of oriented water dipoles that will persist in its direction of orientation for a long time on the scale of molecular motion, perhaps until affected by another ion. The energy to point this array in the opposite direction (in the absence of ionized waters, this would occur by physical rotation of the waters) might possibly be large enough to temporarily discriminate against the next ion coming in from the left. Conversely, an ion approaching from the right side would find an energetically favorable array of dipoles already waiting to assist its solvation into the channel interior. However, given the experience of water molecules flipping spontaneously in a matter of picoceconds as depicted in Fig. 13, it appears that thermal energy is adequate to accomplish the reorientation. Nonetheless, analytic calculations for multiple-ion occupancy models may be in error by assuming that the dielectric environment of the channel interior can be modeled as a uniform constant, ignoring the competition for water orientation by the different ions.

Check of the Water-Peptide Potential. The water-peptide structure we observe inside the channel is subject to uncertainty since the water-peptide potential surface is not well tested. If the water-water hydrogen bonds we have used are too strong compared with the carbonyl-water hydrogen bonds, then this water structure might be an artifact. To investigate the dependence of the water structure on the potentials used, the hydrogen-bond potential energy between water and peptide groups is varied from 14–40 kJ/mol (the unadjusted value for this potential surface being ~22 kJ/mol) leaving all other interactions the same. Depending on precisely how the variation is performed, several effects are observed.

The scaling of the hydrogen-bond energy can be approached in two ways. First, the relative strength of all eight pairwise interactions involved (N—O_W, N—H_W, H—O_W, H—H_W, C—O_W, C—H_W, O—O_W, and O—H_W, where N is the amide nitrogen, H is the amide hydrogen, C is the carbonyl carbon, O is the carbonyl oxygen, O_W is the water oxygen, and H_W is the water hydrogen) can be scaled together so that decreasing the attractiveness of the O—H_W interaction also decreases the repulsion of the O—O_W pair. It is observed in this approach that there is no significant change in either the linear structure of the channel waters or in the dynamics over the range of the adjustments.

A second approach is to only adjust the two interactions, O—H_W and H—O_W. This approach has severe consequences, even for 5% changes in the bond energy. For adjustments resulting in a weaker bond, the waters actually move out of the pore, repulsed by the unadjusted and now overwhelmingly repulsive interactions among the O—O_W and C—H_W pairs. Making the bond stronger causes the waters to become tightly bound to the interior surface of the pore, so much so that waters pack more densely and double up in the pore, completely disrupting the single-file nature of the previous linear structure and severly distorting the peptide as well. Again, the unadjusted O—O_W and C—H_W interactions are now overwhelmed by the proportionately stronger O—H_W interaction. This experience is recounted both to emphasize the sensitivity and multidimensionality of nonbonded potentials (especially ones involved in hydrogen bonds) and to illustrate how important accurate potentials are to the proper simulation of a molecular system. Given the sensitivity and uncertainty of these potentials, any agreement between reality and the present simulation may indeed be fortuitous. In fact, a valuable test of this aspect of the potential surface is whether water and ion structures such as we describe can be observed experimentally (perhaps in higher resolution x-ray data).

Future Research Needed

Much additional research is needed to understand the detailed mechanism of ion transport through even this simplest of biological channels. The obvious shortcomings of the present study include uncertainties in potentials, the lack of free-energy calculations, the omission of lipid and bulk-water phases, and the relatively short simulation times. In addition, we need to probe much more of the channel interior. Although we have examined four different ions, we have observed them in only two localized sections of the channel.

While we are extending our simulations to include these areas, such calculations are extremely demanding computationally and may require up to several months of computer time even on a dedicated array processor (39). Ideally, one would like to map out the free energy, diffusion rate, and perhaps force correlations vs. ion position in the gramicidin channel as a function of ion type, number of ions present, and chemical structure (e.g., amino acid sequence) of the pore. Progress in these areas would permit, for example, the investigation of proposed binding sites within the channel (11, 12, 13, 65) and comparison with the detailed experimental data available on ion conductivity vs. ion concentration and type (2, 11), applied voltage (68, 69), and altered amino acid sequence (63). As detailed structural information becomes available for other ion channels in addition to gramicidin, comparison can be made with similar calculations on the more complex channels in order to discover to what extent gramicidin can validly serve as a general model of ion transport.

CONCLUSION

These initial molecular dynamics computations provide interesting insights into the possible structure and dynamics of ion transport in gramicidin A, including the detailed structure of ion solvation in the channel and a qualitative picture of both peptide flexibility and solvent mobility. Limitations of these calculations include (*a*) relatively imprecise knowledge of the potential surface, (*b*) short simulation times, and (*c*) omission of bulk lipid and water interactions. Therefore, our conclusions should be taken more as speculations that should be further checked against both experimental measurements and more refined and extensive calculations. With these caveats in mind, the calculations indicate that ions are thermodynamically accommodated in gramicidin via several mechanisms: (*a*) by the flexibility of the peptide helix allowing the carbonyl groups in the pore wall to bend inward to solvate the ion, (*b*) by the increased flexibility of the solvating carbonyl groups at the center of the dimer channel due to a break in the covalent structure and perhaps to the smaller amino acid side chains, and (*c*) by the special solvation properties of linear water.

In principle, the molecular dynamic techniques illustrated here can be extended to calculate free energy (60,62), diffusion constant, and force correlation profiles of ions as a function of position in the pore and thus to compare calculated mobilities and diffusion rates with experimental measurements as a function of ion type and concentration, voltage, and amino acid sequence.

APPENDIX

This section describes the potentials and parameters used in the simulations. A particular atom can be described in terms of its individual atomic character (mass, potential energy of interaction with other atoms) and its bondedness to neighboring atoms. To simplify bookkeeping, it is customary to assign a mnemonic label or atom type to every unique combination of such properties that occurs in the system of interest. For most atoms, atomic number alone is not a sufficient criteria by which to classify unique classes of interactions. Therefore, we use a notation that begins with a single letter field specifying the atomic number (e.g., C for carbon) followed by a mnemonic field, which suggests the unique property that distinguishes it from other atoms of the same atomic number. For example, H_HOL is an atom type with the atomic number of hydrogen and with the bonded and electrostatic properties of hydrogen in the alcohol functional group. An underscore is used to separate the two fields for clarity. These labels are only meant to facilitate recognition. The ultimate criteria for how a given atom interacts with its environment is defined by the potential parameters in the following tables.

Table III contains the mnemonic name assignments for the gramicidin model simulated. Each amino acid is defined separately and to aid in the specific assignment of a given atom, connectivity information is provided in the index column. The value of the index is the relative offset necessary to find the atom in the list to which it is bonded. Thus, the third atom in the glycine list, C_GLY, has an index value of −2 and, therefore, is bonded to the atom two lines above it, N_PEP. An index value of 0 means that this atom begins the molecule. The first atom (for all but the formyl

TABLE III
AMINO ACID ATOM ASSIGNMENTS FOR GRAMICIDIN A

Atom type	Index	Atom type	Index	Atom type	Index	Atom type	Index
Formyl		Ethanolamine		Glycine		Tryptophan	
H_AROM	0	N_REP	−2	N_PEP	−2	N_PEP	−2
C_NYL	−1	H_AMIDE	−1	H_AMIDE	−1	H_AMIDE	−1
O_NYL	−1	C_SECOND	−2	C_GLY	−2	C_ALPHA	−2
Leucine		H_ALK	−1	H_ALK	−1	H_ALK	−1
N_PEP	−2	H_ALK	−2	H_ALK	−2	C_SECOND	−2
H_AMIDE	−1	C_SECOND	−3	C_NYL	−3	H_ALK	−1
C_ALPHA	−2	H_ALK	−1	O_NYL	−1	H_ALK	−2
H_ALK	−1	H_ALK	−2	Valine		C_5INDOLE	−3
C_SECOND	−2	O_HOL	−3	N_PEP	−2	C_5INDOLE	−1
H_ALK	−1	H_HOL	−1	H_AMIDE	−1	H_AROM	−1
H_ALK	−2	Alanine		C_ALPHA	−2	N_PYRROLE	−2
C_TERT	−3	N_PEP	−2	H_ALK	−1	H_AMIDE	−1
H_ALK	−1	H_AMIDE	−1	C_TERT	−2	C_5INDOEL	−2
C_PRIM	−2	C_ALPHA	−2	H_ALK	−1	C_5INDOLE	−1,−6
H_ALK	−1	H_ALK	−1	C_PRIM	−2	C_AROM	−1
H_ALK	−2	C_PRIM	−2	H_ALK	−1	H_AROM	−1
H_ALK	−3	H_ALK	−1	H_ALK	−2	C_AROM	−2
C_PRIM	−6	H_ALK	−2	H_ALK	−3	H_AROM	−1
H_ALK	−1	H_ALK	−3	C_PRIM	−6	C_AROM	−2
H_ALK	−2	C_NYL	−6	H_ALK	−1	H_AROM	−1
H_ALK	−3	O_NYL	−1	H_ALK	−2	C_AROM	−2,−8
C_NYL	−15			H_ALK	−2	H_AROM	−1
O_NYL	−1			C_NYL	−12	C_NYL	−20
				O_NYL	−1	O_NYL	−1

group) is the amide nitrogen of a peptide bond and is bonded to the second atom from the end of the adjacent residue in a daisy chain manner.

For biopolymer systems, these unique atom types can become very numerous and unwieldy. To efficiently organize the many atom types, an equivalence table can be implemented by which different atom types that share common sets of parameters for particular interactions are mapped into a common equivalent type. For example, although we must define many subtly different varieties of carbon to account for the various bonding arrangements and vibrational frequencies, we treat most all of them equivalently for the Lennard-Jones pairwise potential energy calculations.

In the equivalence table found in Table IV all the unique atom types necessary to describe the gramicidin systems used in this study along with their equivalence types for the various types of interactions specified in Eq. 1 are listed. In the subsequent tables are the particular parameters for the subset of equivalence types for each of the types of interactions. Thus, to determine the Lennard-Jones parameters that are used for the alpha carbon of tryptophan, first look up in Table III the atom type name of the alpha carbon in tryptophan (which is C_ALPHA), then consult the equivalence table (Table IV) for the equivalent Lennard-Jones type for C_ALPHA (which is C_GLY), and finally look up the C_GLY parameters in the Lennard-Jones table (Table V).

The Lennard-Jones parameters given in Table V are taken from various sources (see the Method section) and are assumed to be transferable, i.e., the parameters are those for a pair of equivalent atoms and the appropriate values for a pair of nonequivalent atoms are determined using a geometric weighting (47) of the two appropriate equivalent pair parameters. The water oxygens are an exception. The water-ion interaction parameters are borrowed from an ion in water simulation (48) and they do not match well the water-water transferable parameters derived by Berendsen et al. (45). Therefore, both sets are used in their respective interactions in the current simulation. The units for ϵ are given in joules per mole, while the units for σ are in ångströms.

The coulombic parameters in Table VI are given in units in coulombs. Note that several of the equivalent coulombic atom types in the equivalence table are multiplied by an integer. This means that the equivalent charge must be scaled first by the given factor before being used for that

TABLE V
LENNARD-JONES PARAMETERS
$4\epsilon[(\sigma/r_{ij})^{12} - (\sigma/r_{ij})^{6}]$

Atom types	σ	ϵ
	Å	*J/mol*
Oxygen*	3.166	650.2
Oxygen‡	3.010	316.8
Hydrogen	0.0	0.0
H_AMIDE	0.0	0.0
H_ALK	2.450	159.0
C_GLY	3.875	163.2
C_NYL	3.617	619.2
O_NYL	2.860	954.0
N_PEP	3.501	698.7
Lithium	2.37	149.3
Sodium	2.73	187.6
Potassium	3.36	588.9
Cesium	3.92	1116.7

*Parameters for water oxygens when interacting with other water and peptide atoms.
‡Parameters for water oxygens when interacting with ions.

TABLE IV
EQUIVALENCE TABLE

Atom types	Equivalent atom types for different interactions				
	Lennard-Jones	Coulombic	Bond length	Bond angle	Torsion angle
Water atoms					
Oxygen	Oxygen	Hydrogen × (−2)	Oxygen	Oxygen	na*
Hydrogen	Hydrogen	Hydrogen	Hydrogen	Hydrogen	na
Peptide atoms					
H_AMIDE	H_AMIDE	H_AMIDE	H_AMIDE	H_AMIDE	H_AMIDE
H_ALK	H_ALK	H_ALK	H_ALK	H_ALK	H_ALK
H_AROM	H_ALK	H_AROM	H_ALK	H_ALK	H_ALK
H_HOL	H_AMIDE	C_NYL	H_HOL	H_HOL	H_HOL
C_PRIM	C_GLY	H_ALK × (−3)	C_PRIM	C_PRIM	C_PRIM
C_SECOND	C_GLY	H_ALK × (−2)	C_PRIM	C_PRIM	C_PRIM
C_TERT	C_GLY	H_ALK × (−1)	C_PRIM	C_PRIM	C_PRIM
C_ALPHA	C_GLY	H_ALK × (−1)	C_PRIM	C_PRIM	C_GLY
C_GLY	C_GLY	H_ALK × (−2)	C_PRIM	C_PRIM	C_GLY
C_AROM	C_NYL	H_AROM	C_AROM	C_AROM	C_AROM
C_5INDOLE	C_NYL	H_AROM	C_5INDOLE	C_5INDOLE	C_AROM
C_NYL	C_NYL	C_NYL	C_NYL	C_NYL	C_NYL
O_NYL	O_NYL	C_NYL × (−1)	O_NYL	O_NYL	O_NYL
O_HOL	O_NYL	C_NYL × (−1)	O_HOL	O_HOL	O_HOL
N_PEP	N_PEP	H_AMIDE × (−1)	N_PEP	N_PEP	N_PEP
N_PYRROLE	N_PEP	H_AMIDE × (−1)	N_PEP	N_PEP	N_PYRROLE
Ions					
Lithium	Lithium	Lithium	na	na	na
Sodium	Sodium	Lithium	na	na	na
Potassium	Potassium	Lithium	na	na	na
Cesium	Cesium	Lithium	na	na	na

*Na, not applicable.

TABLE VI
COULOMBIC PARAMETERS $q_i q_j / r_{ij}$

Atom types	q_i
	$C^* \times 10^{-19}$
Hydrogen	0.657
H_AMIDE	0.449
H_ALK	0.160
H_AROM	0.0
C_NYL	0.609
Lithium	1.602

*Coulomb.

atom type. This is meant to imply that local groups (like a methyl group) have a discrete net coulombic charge (usually zero).

The remainder of the tables (VII–IX) contain parameters for internal (bonded) interactions. The internal water potential parameters have been excluded as they are considerably more complex and can be found elsewhere (49). All of the parameters in Tables VII–IX have been derived from empirical least-square fits to experimental data by one of the authors (A. Hagler). The order of the atom types in the bond angle table, Table VIII, assumes that atom 2 is the central atom. The order of the atom types in Table IX is as they would occur in the molecule, i.e., the

TABLE VII
BOND LENGTH PARAMETERS $K_b(r - r_{eq})^2$

Atom types		K_b	r_{eq}
Atom 1	Atom 2		
		$(Jm^{-2} mol^{-1}) \times 10^{-22}$	$\AA$
H_ALK	C_PRIM	1.423	1.105
H_ALK	C_AROM	1.495	1.105
H_ALK	C_5INDOLE	1.495	1.105
H_ALK	C_NYL	1.423	1.105
H_HOL	O_HOL	2.305	0.960
H_AMIDE	N_PEP	2.023	1.026
C_PRIM	C_PRIM	1.357	1.526
C_PRIM	C_5INDOLE	1.409	1.510
C_PRIM	C_NYL	1.184	1.520
C_PRIM	N_PEP	1.580	1.460
C_PRIM	O_HOL	1.607	1.420
C_AROM	C_AROM	2.276	1.370
C_AROM	C_5INDOLE	1.841	1.370
C_5INDOLE	C_5INDOLE	1.841	1.370
C_5INDOLE	N_PEP	2.259	1.280
C_NYL	N_PEP	1.623	1.320
O_NYL	C_NYL	2.574	1.230

TABLE VIII
BOND ANGLE PARAMETERS $K_\theta(\theta - \theta_{eq})^2$

Atom types			K_θ	θ_{eq}
Atom 1	Atom 2	Atom 3		
			$kJ\ mol^{-1}\ deg^{-2}$	deg
C_PRIM	C_PRIM	C_PRIM	195.0	110.5
H_ALK	C_PRIM	C_PRIM	185.8	110.0
H_ALK	C_PRIM	C_5INDOLE	185.8	110.0
C_PRIM	C_PRIM	C_NYL	195.0	110.5
H_ALK	C_PRIM	C_NYL	188.3	109.5
H_ALK	C_PRIM	H_ALK	165.3	106.4
C_NYL	C_PRIM	N_PEP	209.2	109.5
C_PRIM	C_PRIM	N_PEP	209.2	109.5
H_ALK	C_PRIM	N_PEP	215.5	109.5
C_PRIM	C_PRIM	O_HOL	209.2	105.5
H_ALK	C_PRIM	O_HOL	238.5	109.5
C_AROM	C_AROM	C_AROM	439.3	120.0
H_ALK	C_AROM	C_AROM	146.4	120.0
C_AROM	C_AROM	C_5INDOLE	397.5	120.0
H_ALK	C_AROM	C_5INDOLE	104.6	120.0
C_5INDOLE	C_5INDOLE	C_5INDOLE	397.5	120.0
C_AROM	C_5INDOLE	C_5INDOLE	397.5	120.0
C_PRIM	C_5INDOLE	C_5INDOLE	225.9	120.0
H_ALK	C_5INDOLE	C_5INDOLE	83.7	120.0
C_5INDOLE	C_5INDOLE	N_PEP	414.2	120.0
C_AROM	C_5INDOLE	N_PEP	414.2	120.0
H_ALK	C_5INDOLE	N_PEP	108.8	120.0
C_PRIM	C_NYL	N_PEP	223.8	114.1
O_NYL	C_NYL	N_PEP	284.5	120.0
H_ALK	C_NYL	N_PEP	284.5	120.0
C_PRIM	C_NYL	O_NYL	284.5	120.0
H_ALK	C_NYL	O_NYL	284.5	120.0
H_HOL	O_HOL	C_PRIM	244.8	106.0
H_AMIDE	N_PEP	C_PRIM	146.4	122.0
C_5INDOLE	N_PEP	C_5INDOLE	313.8	120.0
H_AMIDE	N_PEP	C_5INDOLE	83.7	120.0
C_PRIM	N_PEP	C_NYL	464.4	118.0
H_AMIDE	N_PEP	C_NYL	156.9	115.0

TABLE IX
TORSIONAL PARAMETERS $K_\phi[1 + \alpha \cos(n\phi)]$

Atom types				K_ϕ	α	n
Atom 1	Atom 2	Atom 3	Atom 4			
				kJ/mol		
H_ALK	C_PRIM	O_HOL	H_HOL	0.543	1	3
C_PRIM	C_PRIM	O_HOL	H_HOL			
H_ALK	C_AROM	C_AROM	H_ALK	15.5	−1	2
H_ALK	C_AROM	C_AROM	C_PRIM			
H_ALK	C_AROM	C_AROM	C_AROM			
H_ALK	C_AROM	C_AROM	N_PYRROLE			
C_PRIM	C_AROM	C_AROM	N_PYRROLE			
C_AROM	C_AROM	C_AROM	C_PRIM			
C_AROM	C_AROM	C_AROM	C_AROM			
C_AROM	C_AROM	C_AROM	N_PYRROLE			
H_ALK	C_AROM	N_PYRROLE	H_AMIDE	8.37	−1	2
H_ALK	C_AROM	N_PYRROLE	C_AROM			
C_AROM	C_AROM	N_PYRROLE	H_AMIDE			
C_AROM	C_AROM	N_PYRROLE	C_AROM			
H_ALK	C_NYL	N_PEP	H_AMIDE	5.02	−1	2
C_GLY	C_NYL	N_PEP	H_AMIDE			
H_ALK	C_NYL	N_PEP	C_GLY	13.4	−1	2
C_GLY	C_NYL	N_PEP	C_PRIM			
C_GLY	C_NYL	N_PEP	C_GLY			
O_NYL	C_NYL	N_PEP	H_AMIDE	7.5	−1	2
O_NYL	C_NYL	N_PEP	C_PRIM	15.9	−1	2
O_NYL	C_NYL	N_PEP	C_GLY			

angle, ϕ, is that angle formed by the bond connecting atoms 1 and 2 and the bond connecting atoms 3 and 4 looking down the bond of atoms 2 and 3. The value of n determines the number of periods in the torsional potential and hence gives rise to the hybridization state of the bond. The value of α defines the phase of the potential, i.e., whether the minimum occurs with the molecules in a staggered or eclipsed conformation.

We thank the National Institutes of Health, both General Medical Sciences and the Division of Research Resources, the Office of Naval Research, Chemistry, and the National Science Foundation, Chemistry, for providing the support that has made this work possible.

We are indebted to Professor O. S. Andersen for helpful discussions in comparing these calculations with the experiment.

Received for publication 30 September 1983 and in final form 3 April 1984.

REFERENCES

1. Urry, D. W. 1979. Molecular perspectives of monovalent cation selective transmembrane channels. *Int. Rev. Neurobiol.* 21:311–334.
2. Hladky, S. B., and B. W. Haydon. 1972. Ion transfer across lipid membranes in the presence of gramicidin A. I. Studies of the unit conductance channel. *Biochim. Biophys. Acta.* 274:294–312.
3. Kolb, H.-A., and E. Bamberg. 1977. Influence of membrane thickness and ion concentration on the properties of the gramicidin A channel — autocorrelation, spectral power density, relaxation and single-channel studies. *Biochim. Biophys. Acta.* 464:127–141.
4. Veatch, W., N. Sarkar, P. K. Mukherjee, D. Langley, H. Paulus, V. T. Ivanov, and E. N. Shepel. 1979. Biological function of gramicidin A. Comparison of the effect of linear gramicidin A analogs on membrane per- meability, bacterial sporulation and RNA polymerase. *Proc. Am. Peptide Symp., 6th, Rockford, IL.* 707–710.
5. Fisher, R., and T. Blumenthal. 1982. An interaction between gramicidin and the σ subunit of RNA polymerase. *Proc. Natl. Acad. Sci. USA.* 79:1045–1048.
6. Andersen, O. S. 1984. Gramicidin. *Annu. Rev. Physiol.* In press.
7. Rosenberg, P. A., and A. Finkelstein. 1978. Water permeability of gramicidin A-treated lipid bilayer membranes. *J. Gen. Physiol.* 72:341–350.
8. Rosenberg, P. A., and A. Finkelstein. 1978. Interaction of ions and water in gramicidin A channels. Streaming potentials across lipid bilayer membranes. *J. Gen. Physiol.* 72:327–340.
9. Levitt, D. G.. 1984. Kinetics of movement in narrow channels. *In* Ion Channels: Molecular and Physiological Aspects. W. D. Stein, editor. Academic Press, Inc., New York. In press.
10. Bamberg, E., and P. Läuger. 1977. Blocking of the gramicidin channel by divalent cations. *J. Membr. Biol.* 35:351–375.
11. Neher, E., J. Sandblom, and G. Eisenman. 1978. Ionic selectivity, saturation, and block in gramicidin A channels. II. Saturation behavior of single channel conductances and evidence for the existence of multiple binding sites in the channel. *J. Membr. Biol.* 40:97–116.
12. Schagina, L. V., A. E. Grinfeldt, and A. A. Lev. 1978. Interaction of cation fluxes in gramicidin A channels in lipid bilayer membranes. *Nature. (Lond.).* 273:243–245.
13. Koeppe, R. E., J. M. Berg, K. O. Hodgson, and L. Stryer. 1979. Gramicidin A crystals contain two cation binding sites per channel. *Nature. (Lond.).* 279:723-725.
14. Veatch, W. R., E. T. Fossel, and E. R. Blout. 1974. The conformation of gramicidin A. *Biochemistry.* 13:5249–5256.
15. Weinstein, S., B. A. Wallace, J. S. Morrow, and W. R. Veatch. 1980.

Conformation of the gramicidin A transmembrane channel. A ^{13}C nuclear magnetic resonance study of ^{13}C-enriched gramicidin in phosphatidylcholine vesicles. *J. Mol. Biol.* 143:1–19.

16. Wallace, B. A. 1983. Gramicidin A adopts distinctly different conformations in membranes and in organic solvents. *Biopolymers.* 22:397–402.
17. Urry, D. W. 1971. The gramicidin A transmembrane channel. A proposed $\pi_{(L,D)}$ helix. *Proc. Natl. Acad. Sci. USA.* 68:672–676.
18. Born, M. 1920. Volumen und Hydratationswärme der Ionen. *Z. Phys.* 1:45–48.
19. Parsegian, V. A. 1975. Ion-membrane interactions as structural forces. *Ann. NY. Acad. Sci.* 264:161–174.
20. Levitt, D. G. 1978. Electrostatic calculations for an ion channel. I. Energy and potential profiles and interactions between ions. *Biophys. J.* 22:209–219.
21. Jordan, P. C. 1981. Energy barriers for passage of ions through channels. Exact solution of two electrostatic problems. *Biophys. Chem.* 13:203–212.
22. Urry, D. W. 1982. On the molecular structure and ion transport mechanism of the gramicidin transmembrane channel. *In* Membranes and Transport. A. N. Martonosi, editor. Plenum Publishing Corp., New York. 2:285–294.
23. Eisenman, G., and J. P. Sandblom. 1984. Modeling the gramicidin channel. Interpretation of experimental data using rate theory. *Biophys. J.* 45:88–90.
24. Sandblom, J., G. Eisenman, and E. Neher. 1977. Ionic selectivity, saturation and block in gramicidin A channels. I. Theory for the electrical properties of ion selective channels having two pairs of binding sites and multiple conductance states. *J. Membr. Biol.* 31:383–417.
25. Urry, D. W., T. L. Trapane, and K. U. Prasad. 1982. Molecular structure and ionic mechanisms of an ion-selective transmembrane channel: monovalent versus divalent cation selectivity. *Int. J. Quantum Chem., Quantum Biol. Symp.* 9:31–40.
26. Läuger, P., W. Stephan, and E. Frehland. 1980. Fluctuations of barrier structure in ionic channels. *Biochim. Biophys. Acta.* 602:167–180.
27. Levitt, D. G. 1982. Comparison of Nernst-Planck and reaction-rate models for multiply occupied channels. *Biophys. J.* 37:575–587.
28. Ovchinnikov, Y. A., and V. T. Ivanov. 1983. Helical structures of gramicidin A and their role in ion channelling. *In* Conformation in Biology. R. H. Sarma, editor. Adenine Press, Guilderland, NY. 155–174.
29. Bamberg, E., H.-J. Apell, H. Alpes, E. Gross, J. L. Morell, J. F. Harbaugh, K. Janko, and P. Läuger. 1978. Ion channels formed by chemical analogs of gramicidin A. *Fed. Proc.* 37:2633–2638.
30. Ramachandran, G. N., and R. Chandrasekharan. 1972. Conformation of peptide chains containing both L- and D-residues. Part I. Helical structures with alternating L- and D-residues with special reference to the LD-ribbon and the LD-helices. *Indian J. Biochem. Biophys.* 9:1–11.
31. Popov, E. M., and G. M. Lipkind. 1979. Conformation and mechanism of functioning of gramicidin A. *Mol. Biol. (Mosc.)* 13:363–376.
32. Venkatram-Prasad, B. V., and R. Chandrasekaran. 1977. Conformation of polypeptide chains containing both L- and D-residues. II. Double-helical structures of poly-LD-peptides. *Int. J. Pept. Protein Res.* 10:129–138.
33. Venkatachalam, C. M., and D. W. Urry. 1984. Theoretical conformation analysis of the gramicidin A transmembrane channel. *J. Comp. Chem.* 5:64–71.
34. Brickmann, J., and W. Fischer. 1983. Entropy effects on the ion-diffusion rate in transmembrane protein channels. *Biophys. Chem.* 17:245–258.
35. Fischer, W., J. Brickmann, and P. Läuger. 1981. Molecular dynamics study of ion transport in transmembrane protein channels. *Biophys. Chem.* 13:105–116.
36. Hagler, A. T., F. Naider, P. S. Stern, and R. Sharon. 1979. Computer simulation of the conformational properties of oligopeptides. Comparison and analysis of experimental results. *J. Am. Chem. Soc.* 101:6842-6852.
37. Stern, P. S., J. M. Becker, M. Chorev, M. Goodman, F. Naider, R. Sharon, and A. T. Hagler. 1979. Computer simulation of the conformational properties of peptides. Comparison and analysis of experimental results. *Proc. Am. Peptide Symp., 6th, Rockford, IL.* 257–267.
38. Wilson, K. R.. 1977. Many-atom molecular dynamics with an array processor. *In* Minicomputers and Large Scale Computations. P. Lykos, editor. American Chemical Society, Washington, DC. 147–170.
39. Berens, P. H., and K. R. Wilson. 1983. Molecular mechanics with an array processor. *J. Comp. Chem.* 4:313–332.
40. Dauber, P., and A. T. Hagler. 1980. Crystal packing, hydrogen bonding and the effect of crystal forces on molecular conformation. *Accounts Chem. Res.* 13:105–110.
41. Hagler, A. T., E. Huler, and S. Lifson. 1974. Energy functions for peptides and proteins. I. Derivation of a consistent force field including the hydrogen bond from amide crystals. *J. Am. Chem. Soc.* 96:5319–5327.
42. Hagler, A. T., and S. Lifson. 1974. Energy functions for peptides and proteins. II. The amide hydrogen bond and calculation of amide crystal properties. *J. Am. Chem. Soc.* 96:5327–5335.
43. Hagler, A. T., S. Lifson, and P. Dauber. 1979. Consistent force field studies of intermolecular forces in hydrogen bonded crystals. II. Comparison of the validity of intermolecular potential functions as applied to amide and carboxylic acid crystals. *J. Am. Chem. Soc.* 101:5122–5130.
44. Lifson, S., A. T. Hagler, and P. Dauber. 1979. Consistent force field studies of intermolecular forces in hydrogen bonded crystals. I. Derivation of an intermolecular force field for the carboxylic group, and the C=O ⋯O hydrogen bond from carboxylic acid crystals. *J. Am. Chem. Soc.* 101:5111–5120.
45. Berendsen, H. J. C., J. P. M. Postma, W. F. van Gunsteren, and J. Hermans. 1981. Interaction models for water in relation to protein hydration. *Jerus. Symp. Quantum Chem. Biochem.* 14:331–342.
46. Jorgensen, W. L. 1982. Revised TIPS for simulations of liquid water and aqueous solutions. *J. Chem. Phys.* 77:4156–4163.
47. Kong, C. L. 1973. Combining rules for intermolecular potential parameters. II. Rules for the Lennard-Jones (12-6) potential and the Morse potential. *J. Chem. Phys.* 59:2464–2467.
48. Heinzinger, K., and P. C. Vogel. 1976. A molecular dynamics study of aqueous solutions. III. A comparison of selected alkali halides. *Z. Naturforsch. Sect. A.* 31:463–475.
49. Watts, R. O. 1977. An accurate potential for deformable water molecules. *Chem. Phys.* 26:367-377.
50. Kuchitsu, K., and Y. Morino. 1965. Estimation of anharmonic potential constants. II. Bent XY_2 molecules. *Bull. Chem. Soc. Jpn.* 38:814–824.
51. Beeman, D. 1976. Some multistep methods for use in molecular dynamics calculations. *J. Comput. Phys.* 20:130–139.
52. Swope, W. C., H. C. Andersen, P. H. Berens, and K. R. Wilson. 1982. A computer simulation method for the calculation of equilibrium constants for the formation of physical clusters of molecules. Application to small water clusters. *J. Chem. Phys.* 76:637–649.
53. Urry, D. W., M. C. Goodall, J. D. Glickson, and D. F. Mayers. 1971. The gramicidin A transmembrane channel. Characteristics of head-to-head dimerized $\pi_{(L,D)}$ helices. *Proc. Natl. Acad. Sci. USA.* 68:1907–1911.
54. Apell, H.-J., E. Bamberg, H. Alpes, and P. Läuger. 1977. Formation of ion channels by a negatively charged analog of gramicidin A. *J. Membr. Biol.* 31:171–188.
55. Bamberg, E., H. Alpes, H.-J. Apell, B. Haerter, M. J. Quelle, and D. W. Urry. 1979. Formation of ionic channels in black lipid mem-

branes by succinic derivatives of gramicidin A. *J. Membr. Biol.* 50:257–270.

56. Beveridge, D. L., M. Mezei, P. K. Mehrotra, R. T. Marchese, G. R.-S. T. Vasu, and S. Swaminathan. 1983. Monte Carlo computer simulation studies of the equilibrium properties and structure of liquid water. *Adv. Chem. Ser.* 204:297–351.
57. Urry, D. W., A. Spisni, M. A. Khaled, M. M. Long, and L. Masotti. 1979. Transmembrane channels and their characterization in phospholipid structures. *Int. J. Quantum Chem., Quantum Biol. Symp.* 6:289–303.
58. Goodfellow, J. M.. 1982. Cooperative effects in water-biomolecule crystal systems. *Proc. Natl. Acad. Sci. USA.* 79:4977–4979.
59. Goodfellow, J. M., J. L. Finney, and P. Barnes. 1982. Monte Carlo computer simulation of water-amino acid interactions. *Proc. R. Soc. Lond. B. Biol. Sci.* 214:213–228.
60. Berens, P. H., D. H. J. Mackay, G. M. White, and K. R. Wilson. 1983. Thermodynamics and quantum corrections from molecular dynamics for liquid water. *J. Chem. Phys.* 79:2375–2389.
61. Reimers, J. R., K. R. Wilson, and E. J. Heller. 1983. A time dependent wave packet approach to thermal equilibrium systems. Electronic spectra. *J. Chem. Phys.* 79:4749–4754.
62. White, G. M., and K. R. Wilson. 1984. Free energy, entropy, and quantum corrections from molecular dynamics for liquid water. *J. Chem. Phys.* In press.
63. Bamberg, E., and K. Janko. 1977. The action of a carbonsuboxide dimerized gramicidin A on lipid bilayer membranes. *Biochim. Biophys. Acta.* 465:486–499.
64. Nagle, J. F., and S. Tristram-Nagle. 1983. Hydrogen bonded chain mechanisms for proton conduction and proton pumping. *J. Membr. Biol.* 74:1–14.
65. Urry, D. W., K. U. Prasad, and T. L. Trapane. 1982. Location of monovalent cation binding sites in the gramicidin channel. *Proc. Natl. Acad. Sci. USA.* 79:390–394.
66. Rahman, A. J. 1966. Liquid structure and self-diffusion. *J. Chem. Phys.* 45:2585–2592.
67. McCammon, J. A., C. Y. Lee, and S. H. Northrup. 1983. Side-chain rotational isomerization in proteins. A mechanism involving gating and transient packing defects. *J. Am. Chem. Soc.* 105:2232–2237.
68. Eisenman, G., B. Enos, J. Haegglund, and J. Sandblom. 1980. Gramicidin as an example of a single-filing ionic channel. *Ann. NY. Acad. Sci.* 339:8–20.
69. Andersen, O. S., and J. Procopio. 1980. Ion movement through gramicidin A channels. On the importance of the aqueous diffusion resistance and ion-water interactions. *Acta Physiol. Scand. Suppl.* 481:27–35.